Supplementary Materials for

Chaperone-mediated autophagy is required for tumor growth

Maria Kon, Roberta Kiffin, Hiroshi Koga,Javier Chapochnick*,Fernando Macian, Lyuba Varticovski, and Ana Maria Cuervo*

The PDF file includes:

Materials and Methods

Animals. Five to seven week old Nu/Nu athymic male mice were purchased from the NCI-Frederick and six to eight-week-old C57BL/6 mice were purchased from Jackson Laboratories. All mice were housed under pathogen-free conditions according to established institutional protocols from the Institutional Animal Care and Use Committees of the Albert Einstein College of Medicine.

Cultured Cells. *Human cancer cell lines* (A549, H460, MCF7, MCF12, SK-Hep1, Huh-7, ARO, WRO, Saos), Lung Fibroblasts, NIH-3T3 and Striatal cell lines were purchased from American Type Culture Collection (Manassas, VA). MEFs were prepared in our laboratory and where indicated transformed at passage 2-4 by transfection with a SV40-T antigen expression vector. Two days after transfection, cells were split at 1:10 dilution for 5 successive passages to select for the transformed cells. Except where indicated, all cells were cultured in a 37^0C incubator with 5% CO_2 in RPMI or DMEM medium (GIBCO) supplemented with 10% heat-inactivated fetal bovine serum (FBS). Human immortalized breast epithelial cell lines (MCF12) were maintained in DMEM medium supplemented with 10% heat-inactivated fetal bovine serum, 0.01mg/ml bovine insulin, 20ng/ml human EGF, 100ng/ml cholera toxin, and 500ng/ml hydrocortisone. To deprive cells of serum, plates were extensively washed with Hanks' balanced salts solution (Invitrogen, Carlsbad, CA) and fresh medium without serum was added. Where indicated cells were treated with 5mM paraquat (PQ) or 50nM thapsigargin (TG).

Chemicals, antibodies and proteins. The antibodies against aldolase, hexokinase, phosphoglycerokinase, and the cytosolic tail of LAMP-2A and LAMP-2B were developed in our laboratory (*S1,S2*). The antibodies against the luminal region of LAMP-2 and LAMP-1 were from the Hybridoma Bank (University of Iowa), against hsc70 from Maine Biotechnology Services Inc., against GAPDH and actin from Abcam, against p53 (DO-1), p21 and Cathepsin D from Santa-Cruz Biotechnologies, against ubiquitin from Invitrogen, against Atg7, LC3, mTOR and

phospho mTOR from Cell Signaling, against Atg5/12 and Beclin from Novus, against Grp94 from Assay Designs, against Bip from BD Transduction, against PKM2 and VDAC from Cell Signaling, against cytochrome c from Pharmingen, against HIF-1α from Thermo Scientific and against p62 from BioMol International. Sources of other reagents were as described previously (*S3*-*S5*). The pancaspase inhibitor ZVAD was from Calbiochem, glutamine from Invitrogen and Pfithirin α and adenosine from Sigma.

Intracellular protein degradation. Confluent cells labelled with [^{3}H]leucine (2μCi/ml) (NEN-PerkinElmer Life Sciences) for 48 hr were extensively washed and maintained in medium with an excess of unlabeled leucine (*S6*). Aliquots of the medium taken at different times were precipitated in trichloroacetic acid and proteolysis measured as the amount of acid-precipitable radioactivity transformed in acid-soluble radioactivity at each time. The amount of proteolysis due to macroautophagy was calculated by treating parallel wells with 20mM 3-methyladenine during the chase period. Macroautophagy was determined as the percentage of lysosomal degradation sensitive to inhibition by 3-methyladenine.

Measurement of CMA activity. *CMA reporter assays:* The photoactivable CMA reporter was constructed by inserting a sequence of 21 amino acids of Ribonuclease A bearing the CMA-targeting motif in the N-terminus multicloning site of the photoactivatable protein mCherry1 (PA-mCherry1 (*S7*)) and the photoswitchable variants by inserting the same sequence in the N-terminus of the photoswitchable cyan fluorescent protein 2 (PS-CFP2) (*S7*). Cells transduced with a lentivirus carrying the KFERQ-bearing constructs were photoactivated by exposure to a 3.5mA (current constant) light emitting diode (LED: Norlux, 405nm) for 10min and at the desired times fixed in 3% formaldehyde and images were captured with an Axiovert 200 fluorescence microscope (Zeiss) equipped with a 63x 1.4 NA oil objective lens and red (ex. 570/30 nm, em. 615/30 nm), cyan (ex. 365/50 nm and em. 530/45 nm) and green (ex. 475/40 nm and em. 535/45 nm) filter sets (Chroma). All images were acquired with a high-resolution CCD camera.

Acquired z-stack images were subjected to deconvolution using an Axio-Vision program (Zeiss) and then prepared using Adobe Photoshop 6.0 software (Adobe Systems). Quantification was performed in individual frames after deconvolution and thresholding using ImageJ software (NIH) in a minimum of 20 cells per slide. *In vitro uptake assay:* Transport of purified proteins into isolated lysosomes was analyzed using a previously described *in vitro* system (*S6*). Briefly, intact lysosomes were incubated with a pool of radiolabeled cytosolic proteins for 20 min at 37ºC. At the end of the incubation, samples were precipitated in acid and filtered. Proteolysis was calculated as the amount of acid precipitable radioactivity (protein) transformed in acid soluble (amino acids) during the incubation.

Lentivirus-mediated shRNA. The sequences of the regions targeted by the siRNA in the exon 10a of the human *LAMP-2A* gene were 5'-GACTGCAGTGCAGATGA-3' and 5'-AAGCACCATCATGCTGGATAT-3', against Atg7 5'-GGTGTTTAACTCTTCACAT-3' and against LAMP-2B 5'-GTGCTGCTGACTCTGACC-3'. The hairpin (sense–loop–antisense) for these sequences was inserted between the blunt-ended BamHI and SalI sites of the pCCL.PPT.hPGK.GFP.Wpre lentiviral transfer vector (*S8*) and lentiviral particles were generated by co-transfection with the third-generation packaging constructs pMDLg/pRRE and pRSV-REV, and as envelope the G glycoprotein of the VSV (pMD2.G) into HEK293T cells as described before (*S3*). Cultured cells were transduced by addition of packed virus at a titter of $2.63x10^6$ units/ml. Where indicated, tumor-bearing mice were monitored periodically and when tumors reached volumes of 100-200 mm^3 they were injected on two consecutive days with $5x10^7$ of lentivirus in ice cold Hank's buffer twice. Tumor growth was measured 2-3 times a week. Stable p53 knockdown (p53KD) isogenic cell line pairs from wild-type p53 (wtp53) expressing H460 cells were generated as described before (*S9*).

Cellular proliferation and viability. The following assays were used to compare rates of proliferation of the different cell types: a) *BdrU incorporation.* Cells were plated in 96-well plates (10,000 cells/well) and 48 hours later, 5-Bromo-2′-deoxy-uridine (BrdU; Roche Biosciences) was

added for 12h. Cells were fixed and immunostained with the anti-BrdU antibody following the manufacturer's instructions. Absorbance was measure at 405nm excitation and 490nm emission in a plate reader (Perkin Elmer) and intensity values were normalized to the cell number at the end of the incubation, determined by hemocytometer cell counting after trypsinization. b) *Clonigenicity***.** Cells were seeded into 96-well plates (0.5 cells/ per well) and after 2 weeks, all wells were fixed and stained with 4% Crystal Violet dye in methanol. The amount of wells that contained expanded clones was counted. The following methods were used to determine changes in cellular viability: a) *Apoptosis* was determined with Annexin V-PE apoptosis detection kit (BD Pharmingen) and cell death by double labeling Annexin V-7AAD (DB Pharmingen) following manufacturer's instructions. Stained cells were analyzed on a FACScan (Beckton-Dickinson). b) *Acridine orange/ethidium bromide* staining was performed with live cells in culture at the concentration of 250ug/ml of each dye and images were captured with an Axiovert 200 fluorescence microscope (Zeiss). Cells were considered late apoptotic if they had a shrunken cytoplasm and nucleus and a condensed chromatin (visualized in green by acridine orange), as well as positive for the red ethidium bromide staining. Cellular cell cycle distribution was determined by FACS in cells fixed in 70% ethanol and resuspended in 1 ml of FACS solution (PBS, 0.1 % TritonX-100, 500 μg/ml propidium iodide (Sigma), and 0.2 mg/ml DNase free RNase (Sigma)). After a final incubation at room temperature for 30 min, cells were analyzed using a FACSCalibur flow cytometer (BD Biosciences). Data was analyzed by the FlowJo software (Tree Star, Inc., OR). To determine sensitivity to cellular detachment (anoikis) cells were cultured in polypropylene tubes for 48 hours and the amount of dead cells was assessed by Trypan Blue viability staining.

Metabolic analysis. Intracellular ATP and extracellular secretion of lactate were determined using the ATP Bioluminescence Assay Kit HS II (Roche Diagnostics) and the Lactate Assay Kit (MBL International), respectively. Measurement of extracellular acidification rate (ECAR), as well as oxygen consumption rate (OCR), was performed in XF96 plates using XF Extracellular

Flux Analyzer (Seahorse Bioscience). Cells were seeded into the 96-well XF96 plates at 10,000 cells per well. After the indicated treatments, the extracellular pH and oxygen content were measured in untreated conditions and in the presence of 2μM Rotenone (Sigma), previously determined to induce complete inhibition of mitochondrial phosphorylation. This treatment allowed for measurement of lactate generation under basal conditions (mainly resulting from glycolysis and glutaminolysis) and in response to blockage of mitochondria oxidation. The percentage of OCR due to mitochondria oxidation was defined as that sensitive to inhibition with rotenone. Rates of fatty acid β-oxidation were determined by a modification of a previously used method (*S10*). Briefly, the rate of carbon dioxide production from the oxidation of [^{14}C] oleate was measured in cells cultured in the presence of [^{14}C]oleate–BSA complex as the released [14C]carbon dioxide trapped for 1 h at 37 °C onto filter paper soaked in 100mM sodium hydroxide. The rate of β-oxidation was calculated as the amount of trapped [^{14}C]carbon dioxide in relative units produced per mg protein per hour. Mitochondrial oxidative phosphorylation was evaluated after staining of cultured cells for 30 min with the fluorogenic dye MitoSOX^{TM}Red (Invitrogen) that upon oxidation by mitochondria-generated superoxide produces red fluorescence.

Assessment of xenograft tumor growth, cell motility and metastasis. Xenografts of human cancer cells in mice were generated by subcutaneous injection of 1x10^6 cells into their right flank. Tumor growth was measured every 2-3 days with calipers, and tumor volume was calculated by the formula: length x (width)^2 x0.52. At the end of the experiment tumors were excised, fixed in 10% formalin and embedded in paraffin for histological analysis and immunostaining. Cell motility was determined using: 1) *wound closure assay*. Briefly, cells were plated in 6-well plates and grown to confluency. A single scratch was made with a sterile pipette tip and pictures were taken with a phase contrast lens with the Axiovert 200 inverted fluorescence microscope (Zeiss) at different times after wounding. The distance between the leading edges on both sides of the wound was measured at five different points of the wound to

obtain an average value (where indicated, serum was removed from the culture media to avoid filling of the wound through cellular proliferation); and 2) *the trans-well migration assay.* Briefly, 10^5 cells were plated in serum-free medium on top of a 8.0 μm pore membrane insert (BD Falcon) coated with 0.5 mg/ml of Growth Factor Reduced Matrigel Matrix (BD Biosciences) with the lower chamber containing 10 % FBS-supplemented medium. After 48 hours the membranes were fixed in 4 % paraformaldehyde and stained with 0.2 % Crystal Violet dye. The top portion of the membrane was wiped clean and only the cells that migrated through the pores and attached on the bottom side were visualized in an inverted microscope as above. To generate metastasis, a total of $1x10^6$ cells suspended in 100ul of ice-cold Hank's Balanced Salt Solution were injected into the tail vein of 6-8 week old athymic mice. Metastasis from the primary tumor were analyzed after injection of $5x10^5$ cells into the foot fat pad. The lungs of injected animals were collected 3 weeks post-injection, fixed in 10% formalin, and embedded in paraffin for histological analysis and immunostaining. Where indicated, half of the lungs were digested with 1mg/ml Collagenase A (Roche) supplemented with DNAseA for 4 hours at 37ºC, filtered through a mesh and analyzed by FACS for the GFP-positive cells.

Histological Procedures. *Histological staining:* Tumor specimens were fixed in 10% neutral formalin, and 6 μm sections were stained with hematoxylin and eosin. Tissue sections were examined in a blind fashion by a pathologist and graded for the degree of cellular debri and inflammatory cell infiltration. *Terminal Deoxynucleotide Transferase-mediated Deoxyuridine Triphosphate Nick End-labeling (TUNEL) Assay:* The free 3'-OH termini of double or single stranded, low molecular weight DNA fragments, resulting from cleavage of genomic DNA during apoptosis were stained in dewaxed and rehydrated paraffin sections using a commercial kit (Roche Applied Science) according to the manufacturer's instructions. Stained sections were visualized under the fluorescence microscope. *Immunohistochemistry:* Unstained tumor sections were melted at 60^0C for 1 hour, dewaxed in xylene, and rehydrated in 100%, 95%, and 70% ethanol washes. Antigen retrieval was achieved by steaming the slides for 20 minutes and

cooling them in 1mM EDTA pH8 for 20 minutes. Prior to blocking with 2.5% dry milk/2%BSA/0.1%Tween-20 buffer, slides were treated with 0.3% hydrogen peroxide for 10 minutes. After incubation with the desired primary antibody, slides were then extensively washed and upon incubation with fluorescence-conjugated secondary antibodies, they were mounted in SlowFade Gold antifade reagent with DAPI (Invitrogen) and observed on an Axiovert 200 fluorescence microscope (Zeiss). In the case of human tumors paraffin-embedded slices of matched human hepatocellular carcinoma and healthy liver tissue were obtained from the biorepository of the Hepatology Unit of the Dept. of Medicine of the Albert Einstein College of Medicine liver samples and slides from the other healthy tissues and human tumors were obtained from US Biomax, Inc. The slides were heated and dewaxed following standard procedures for epitope retrieval, and then boiled, quenched and blocked before incubation with the desired primary antibodies (*S11*). Primary antibody (anti-human LAMP-2A and LAMP-2B) were used at 1:200 dilutions, and incubated at 4^0C overnight. Rabbit secondary antibody conjugated to Alexa488 was used at 1:300 dilution for 1 hour at room temperature for the liver samples and rabbit secondary antibody conjugated to HRP was used ad 1:300 dilution for 1 hour at room temperature for the rest of tumor samples. To minimize autofluorescence, the liver slides were then incubated with 10mM copper sulfate in 50mM acetate buffer pH5.0 for 1 hr at room temperature. Senescence in cultured cells was assessed by β-Galactosidase expression levels, using the Senescence Kit (BioVision, CA). The images of the stained cells *in vitro* were captured with an Axiovert 200 fluorescence microscope (Zeiss) with the phase filter.

Quantification of mRNA levels. Quantitative real time PCR was used to determine changes in mRNA levels using the TaqMan One-Step RT-PCR Master Mix reagent (Applied Biosystem). Relative transcript levels were analyzed by real-time PCR in 20 µl reaction volume on 96-well plates, using StepOne Plus Real-Time PCR Cycler (Applied Biosystems). The expression levels of LAMP-2A, GAPDH, and 3PGK in different samples were normalized to those of β-actin in the same samples. The following sequences were used for RT-PCR analysis: human LAMP-2A 5'-

TGA CGA CAA CTTCCT TGT GC-3'; human GAPDH: 5'-AAGGTG AAG GTC GGAGT-3'; human 3PGK: 5'- CCT TG AGC CAG TTG CTG T-3' and human β-actin: 5'-GTG CGT GAC ATT AAG GAG AAG CTG-3'.

Statistical analysis. All numerical results are reported as mean+S.E., and represent data from a minimum of three independent experiments unless otherwise stated. We determined the statistical significance of the difference between experimental groups in instances of single comparisons by the two-tailed unpaired Student's t-test of the means with Sigma Plot (Jandel Scientific) software. In instances of multiple means comparisons, we used one-way analysis of variance (ANOVA) followed by the Bonferroni *post-hoc* test to determine statistical significance.

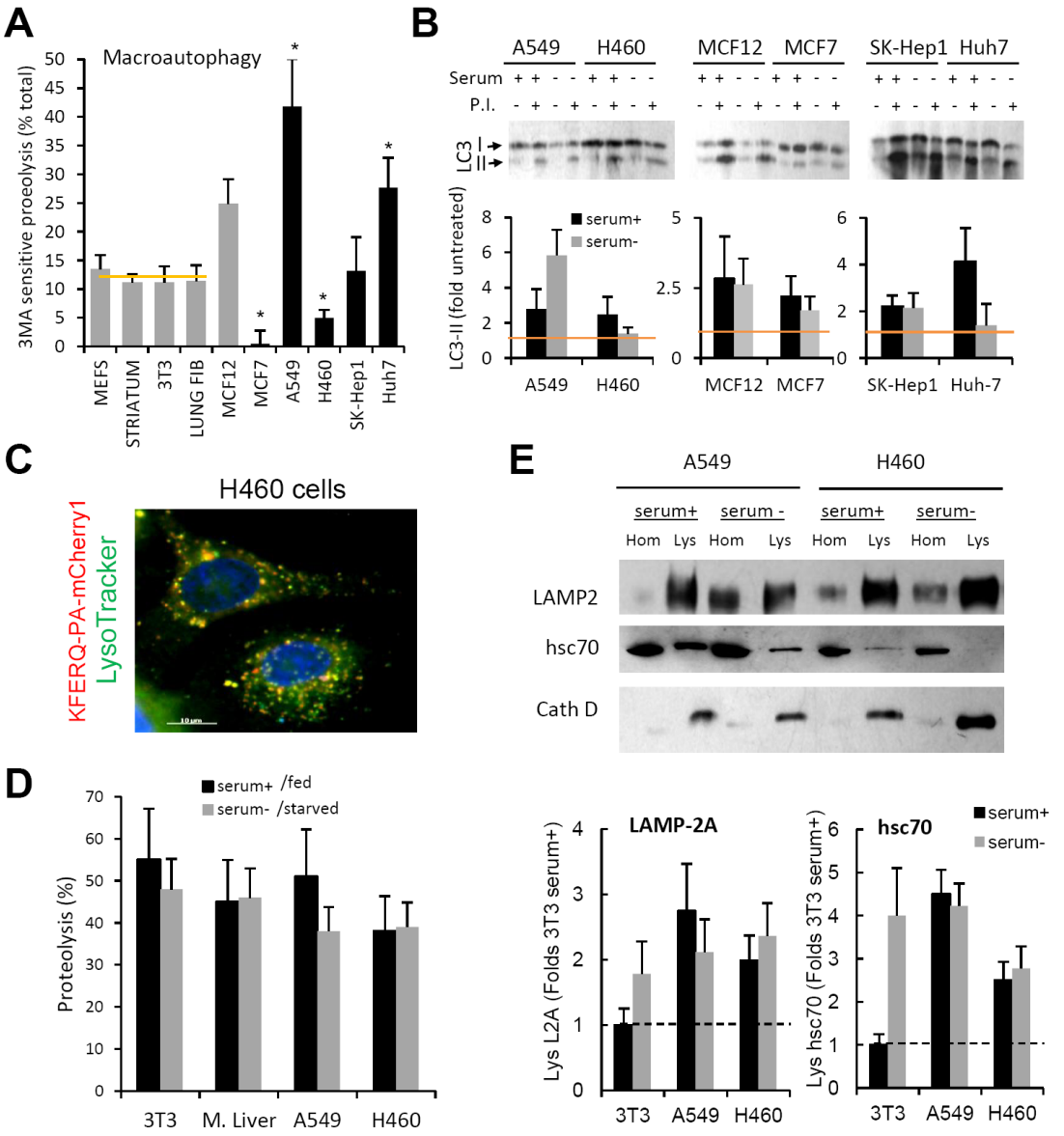

Fig. S1. Autophagic/lysosomal system in human lung cancer cells.
(**A**) Rates of long-lived protein degradation sensitive to 3-methyladenine (macroautophagy) in the indicated non-tumoral (grey) and tumoral (black) cell lines (n= 5-8). Orange line: average value of non-tumoral cells. (**B**) Macroautophagic flux in the 5 tumoral cell lines and in MCF12 as an example of non-tumoral cell line. Top: Representative immunoblots. Bottom: LC3-II flux (n = 4-5). (**C**) Colocalization of the KFERQ-PA-mCherry1 reporter for CMA with the acidic compartment (lysosomes) highlighted with LysoTracker in H460 cells. (**D**) Degradation of a pool of radiolabeled cytosolic proteins by lysosomes isolated from the indicated cells maintained in the presence or absence of serum, or isolated from fed or starved mouse livers. Lysosomes were disrupted by a hypotonic shock to directly analyze their proteolytic capability. Values are from 2 different experiments with triplicate samples. (**E**) Immunoblots of total cellular homogenates (Hom) and lysosomes (Lys) from the same cells. Top: Representative immunoblot. Bottom: Relative values of the levels of LAMP-2A (left) and hsc70 (right) in lysosomes. Values in 3T3 cells in presence of serum were given an arbitrary value of 1 (dotted line). Values are mean + S.E (n =3).

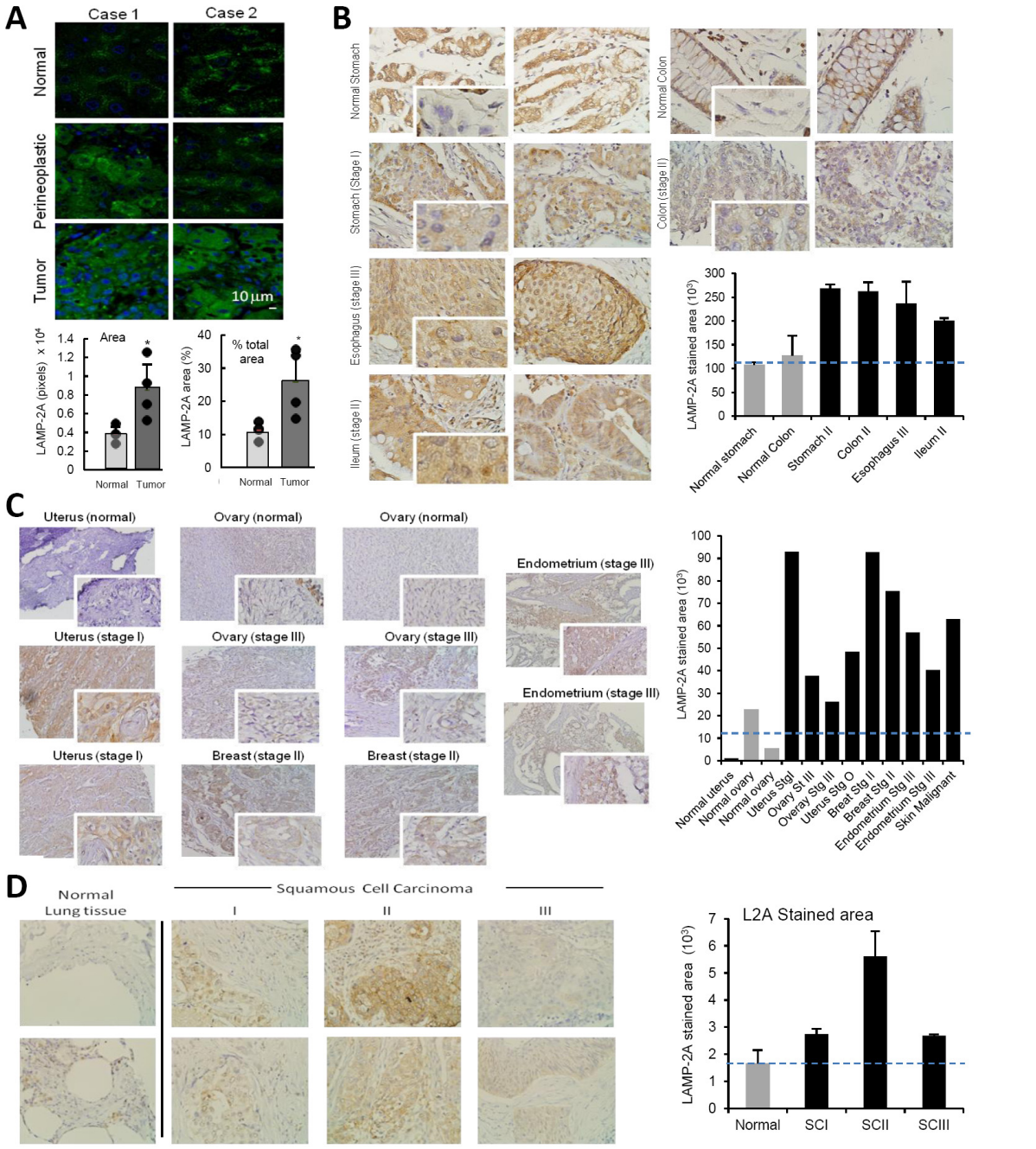

Fig. S2. Levels of LAMP-2A in different types of human cancers.
(**A**) Immunofluorescence staining for LAMP-2A of human hepatocellular carcinomas. Top: example of LAMP-2A staining in livers from two different patients in hepatocarcinoma, perineoplastic regions and lesion-free regions of the same livers. Bottom: Quantification of the total LAMP-2A positive area (left) and percent of cellular area positive for LAMP-2A (right) in normal and tumor human liver regions. Values are mean + S.E. of 5 different patients. Black dots represent the individual values and bars are the mean values. (**B-D**) Immunohistochemistry for LAMP-2A in sections of tumors in the gastrointestinal (**B**) and reproductive (**C**) systems and in lung (**D**) and corresponding normal tissues. Insets show higher magnification regions. Right: Quantification of the LAMP-2A positive area in each individual tumor. When available, stage of the tumor is indicated. Blue dotted lines represent mean value in normal control tissues.

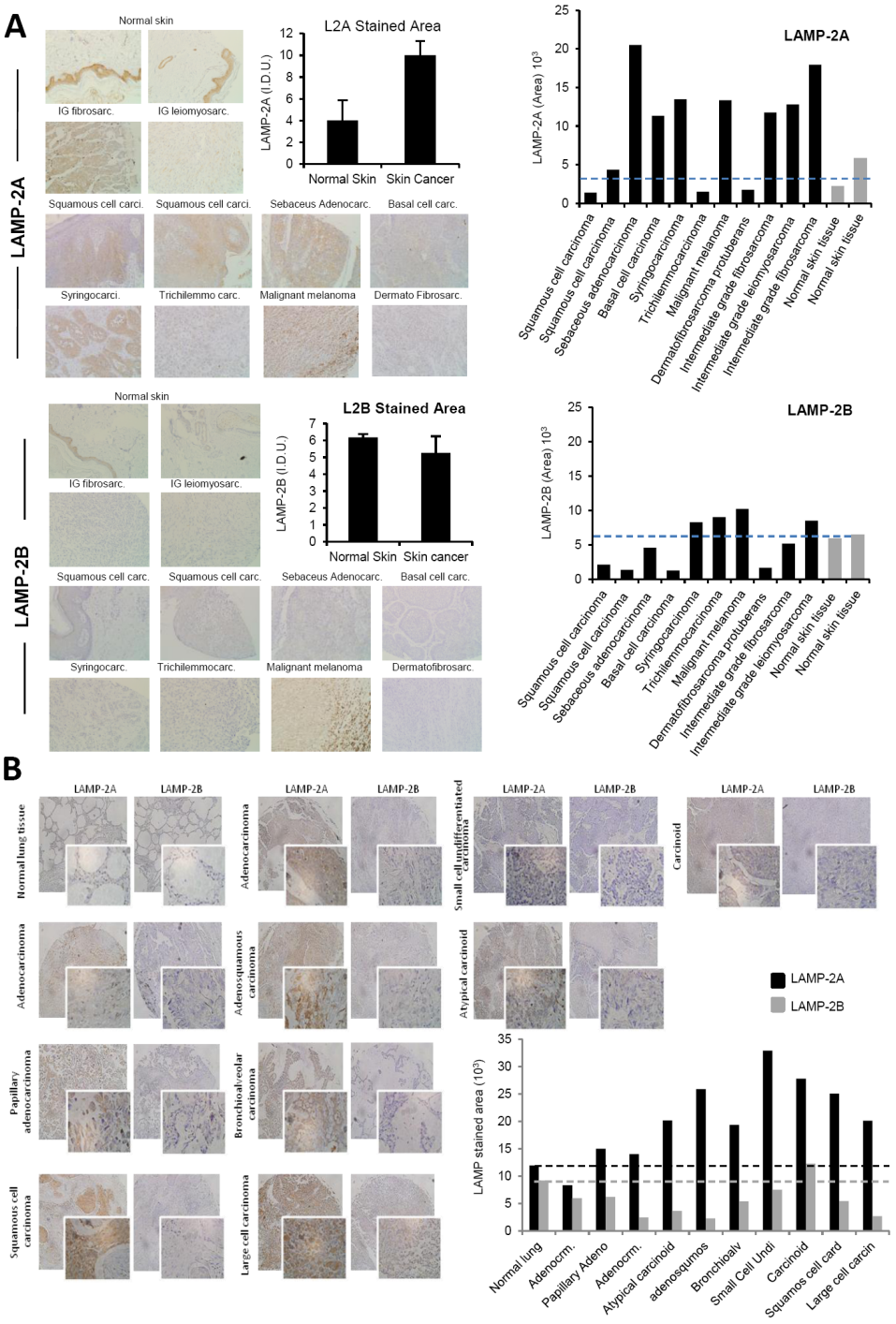

Fig. S3. Immunostaining for LAMP-2A and B in different types of skin and lung human cancers.

Immunohistochemistry for LAMP-2A and LAMP-2B in sections of skin (**A**) and lung (**B**) tumors and corresponding normal tissues. Insets show higher magnification regions. Center: Mean value of the quantification of LAMP-2A and LAMP-2B staining in all normal and cancer samples, as labeled. Right: Quantification of the LAMP-2A and LAMP-2B positive areas in each individual tumor. Blue dotted lines represent mean value in normal control tissues (**A**) and black and grey dotted lines represent mean value for LAMP-2A and LAMP-2B staining, respectively in control tissues (**B**).

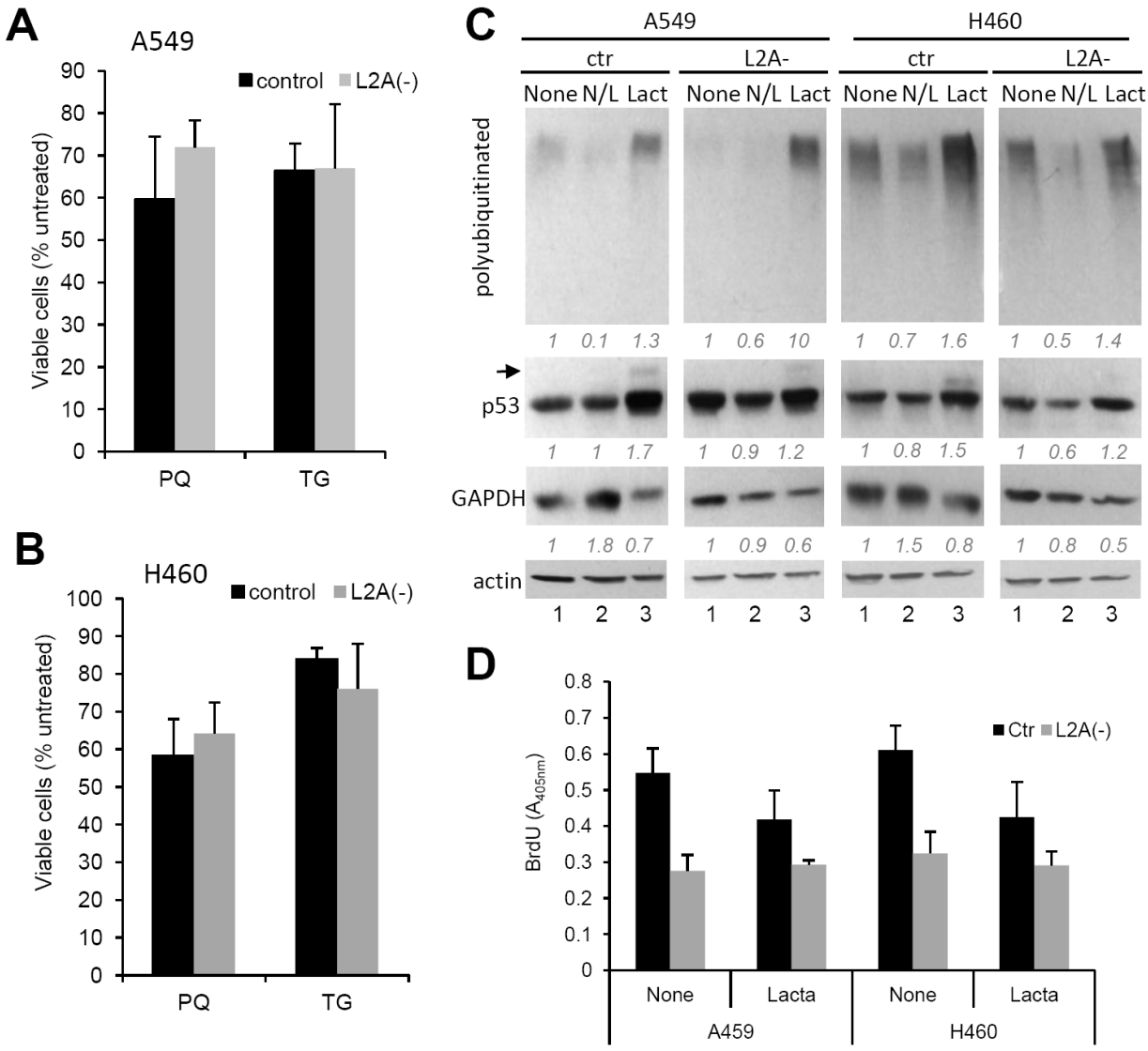

Fig. S4. Effect of CMA blockage on stress resistance and intracellular proteolysis of human lung cancer cells.
Viability of A549 (**A**) and H460 (**B**) cells control or RNAi for LAMP-2A (L2A(-)) 24 h after exposure to 0.5mM paraquat (PQ) or 50nM thapsigargin (TG). Values are mean+S.E. of 3 different experiments with triplicate samples. (**C**) Effect of lysosomal (N/L) and proteasomal (Lact: lactacystin) inhibitors on levels of the indicated proteins in human cancer cell lines control (Ctr) or RNAi for LAMP-2A (L2A-). Numbers in italics indicate folds intensity of untreated samples. (**D**) Effect of treatment with lactacystin on the BrdU incorporation in the same cells. Values are mean+S.E. (n=4-5)

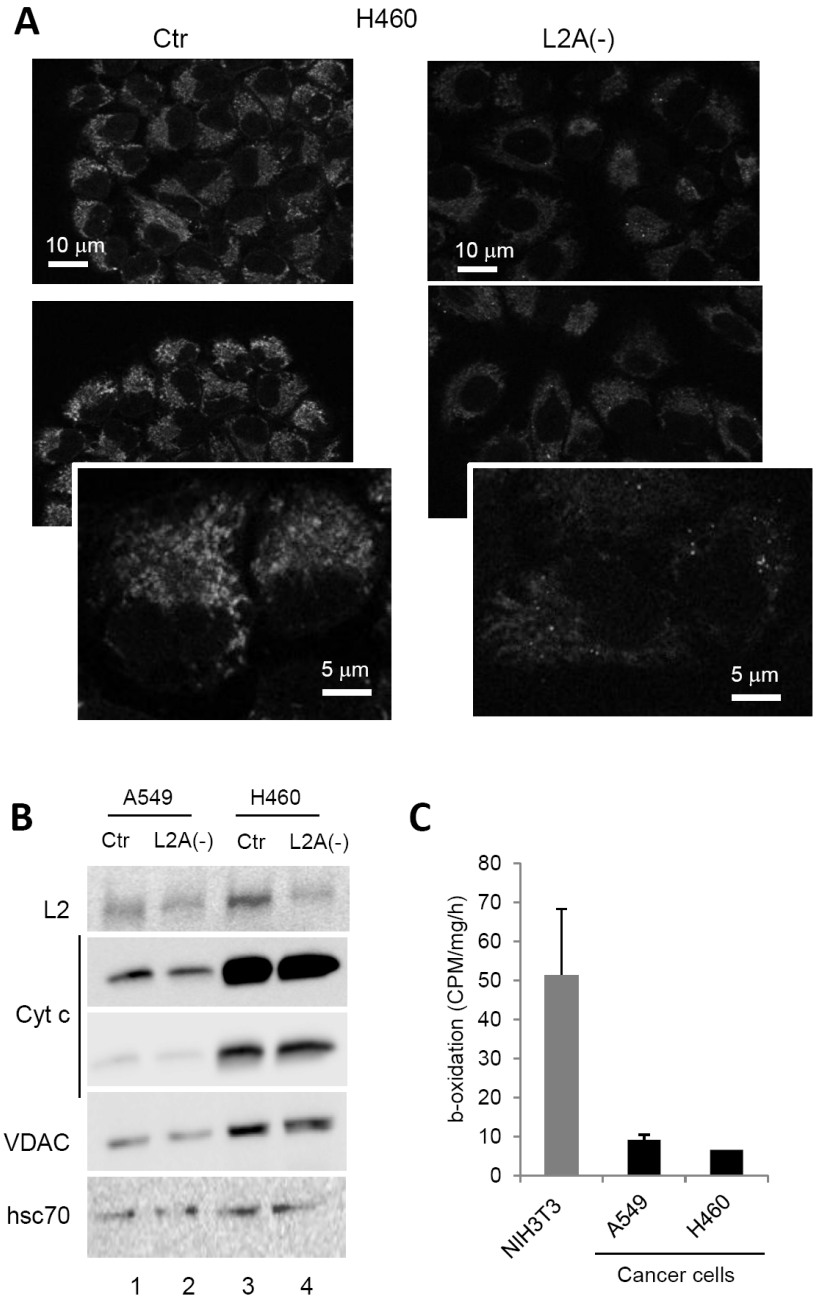

Fig. S5. Effect of CMA blockage on mitochondrial activity and content in human lung cancer cells.
(**A**) MitoSox staining of control (ctr) and LAMP-2A RNAi (L2A(-)) A549 and H460 human lung cancer cells. Insets show higher magnification images. (**B**) Immunoblot for the indicated proteins in the same cells. (**C**) Oxidation of radiolabeled fatty acids in non-tumoral NIH3T3 cells (grey) and two human lung cancer cell lines (black).

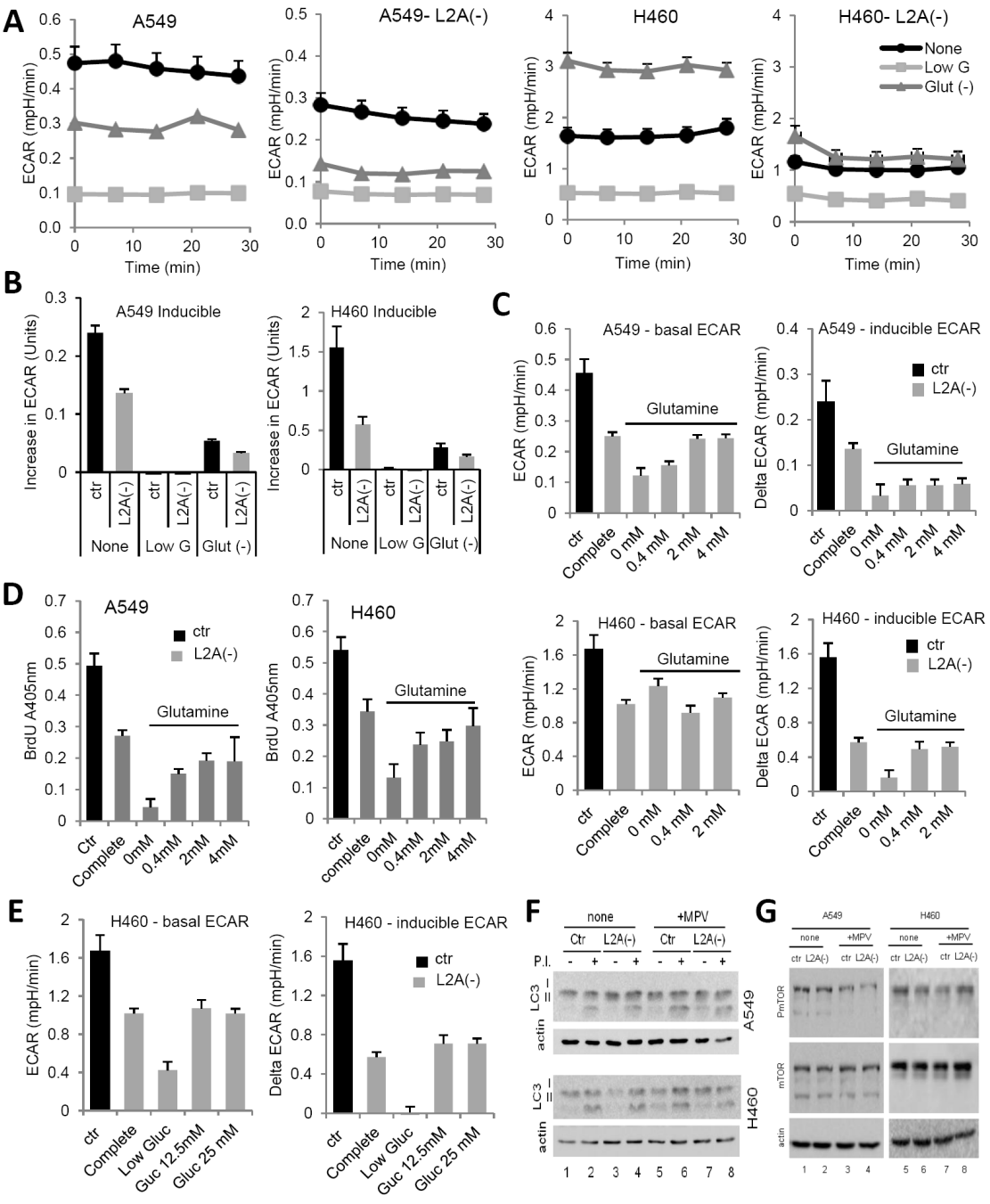

Fig. S6. Metabolic changes in CMA-compromised cancer cells in response to different supplementations.

(**A, B**) Extracellular acidification rates (ECAR) in control (ctr) and LAMP-2A RNAi (L2A(-)) human lung cancer cells maintained in complete media (none), low glucose media (Low G) and media depleted of glutamine (Glut (-)) under basal conditions (**A**) or after addition of rotenone (inducible ECAR) (**B**). (**C, D**) Changes in ECAR (**C**) and in BrdU incorporation (**D**) in the same cells after supplementation with the indicated concentrations of glutamine. (**E**) Changes in ECAR in the same cells maintained in low glucose media or after supplementation with the indicated concentrations of glucose (Gluc). (**F**) LC3-II flux in ctr and L2A(-) human lung cancer cells without additions (none) or in the presence of methylpyruvate (+MPV). (**G**) Immunoblot for the indicated proteins in the same cells. All values are mean+S.E. (n=4-6).

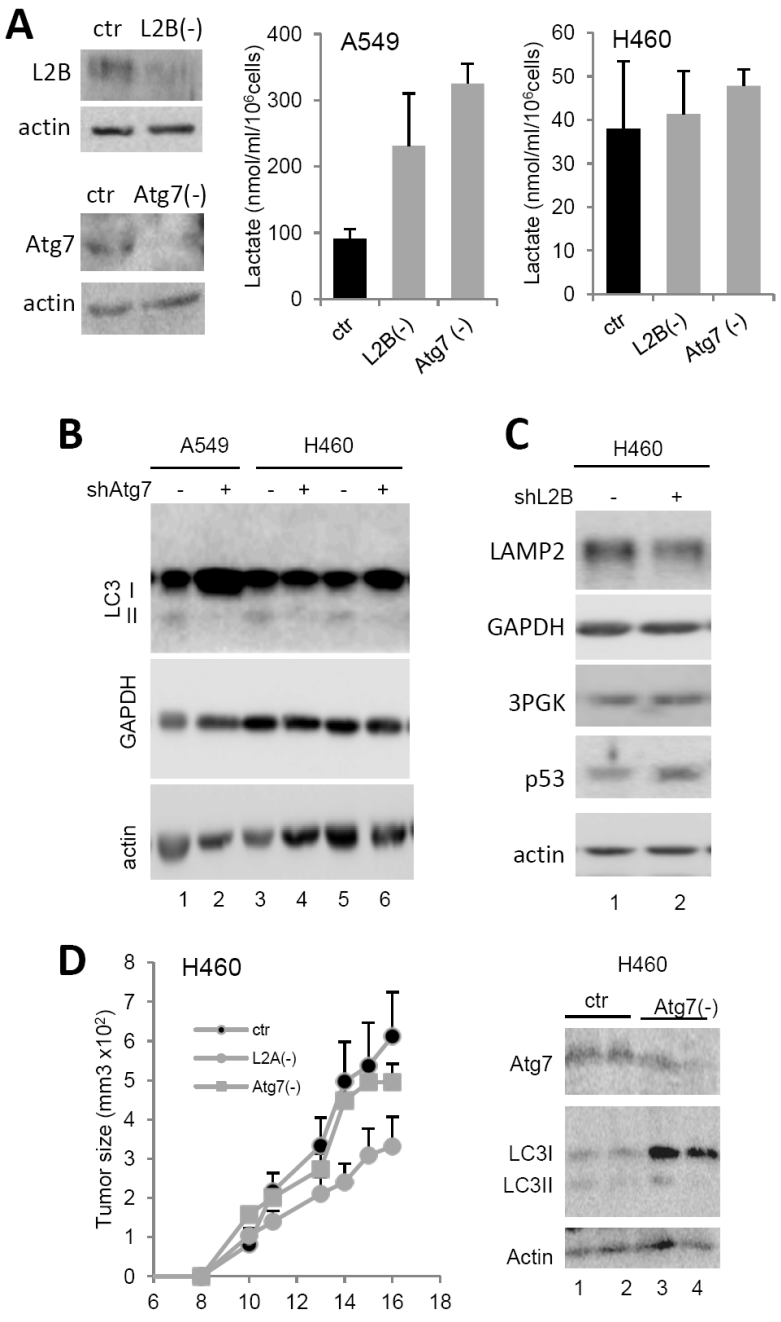

Fig. S7. Effect of genetic blockage of macroautophagy in human lung cancer cells on metabolism and tumor growth.
(**A**) Levels of extracellular lactate in human lung cancer cells control (ctr; black) or RNAi for LAMP-2B (L2B(-);grey) or Atg7 (Atg7(-); grey). Representative immunoblot for the knock-down proteins is shown on the left. (**B, C**) Immunoblot for the indicated proteins in the same cells. (**D**) Growth curves of tumors grown from xenografts of H460 human lung cancer cells control or RNAi for Atg7. Values are mean+S.E. of 4-6 individual tumors. Representative immunoblots of the levels of Atg7 and LC3-II in resected tumors are shown on the right.

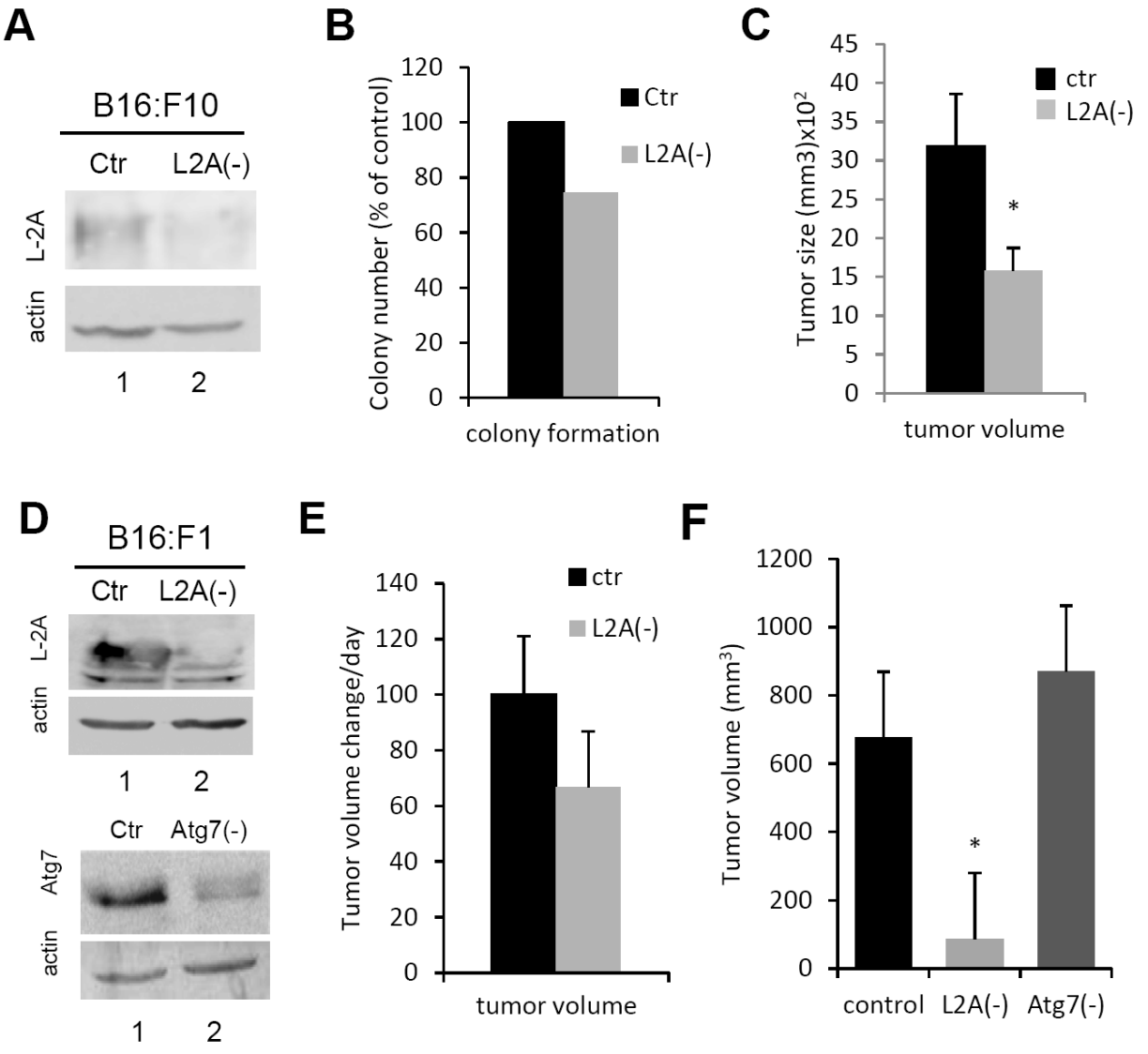

Fig. S8. Effect of CMA blockage on proliferation and melanoma cell tumor growth.
(**A**) Immunoblot for LAMP-2A of B16:F10 melanoma cells control (ctr) or RNAi for LAMP-2A (L2A(-)). (**B**) Ability to form colonies of the same cells. Values are expressed as percentage of plated cells that form colonies. (**C**) Mean maximum size of tumors grown from grafts of the same cells. (**D**) Immunoblots for LAMP-2A and Atg7 of B16:F1 melanoma cells control (ctr) or RNAi for LAMP-2A (L2A(-)) or Atg7 (Atg7(-)). (**E-F**) Average change in volume per day (**E**) and mean maximum size (**F**) of tumors grown from grafts of the same cells (n=6-8).

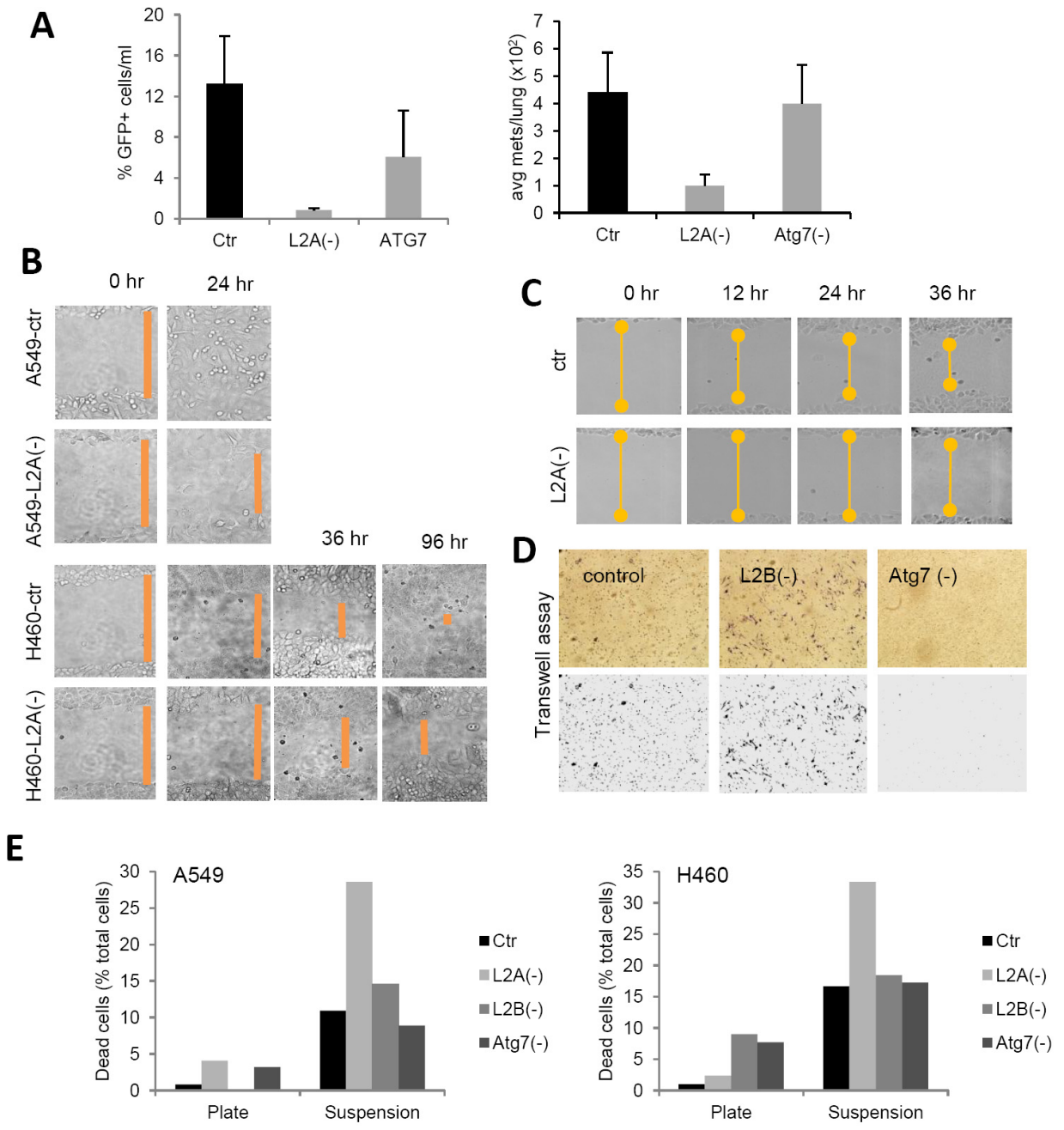

Fig. S9. Effect of macroautophagy and CMA blockage on cancer cell motility and resistance to anoikis.

(**A**) Mouse melanoma cells B16:F1 control (ctr) or RNAi for LAMP-2A or Atg7 were injected in the foot fat pad of mice and the number of cancer cells (detected by FACS analysis as GFP fluroescent cells) (left) and the average number of lung metastasis (right) was quantified (n=4-5). (**B,C**) Time course of wound closing in human lung cancer cells control and interfered for LAMP-2A maintained in the presence (**B**) or absence (**C**) of serum. Notice that the wound in C was double the size to better quantify migration. Connector orange lines mark the borders of the wound. (**D**) Migration of human lung cancer cells control and RNAi for L2B and Atg7 in the trans-well assay. (**E**) Percentage of death cells detected in the plate and in suspension after preventing attachment of human lung cancer cells ctr or RNAi for the indicated proteins.

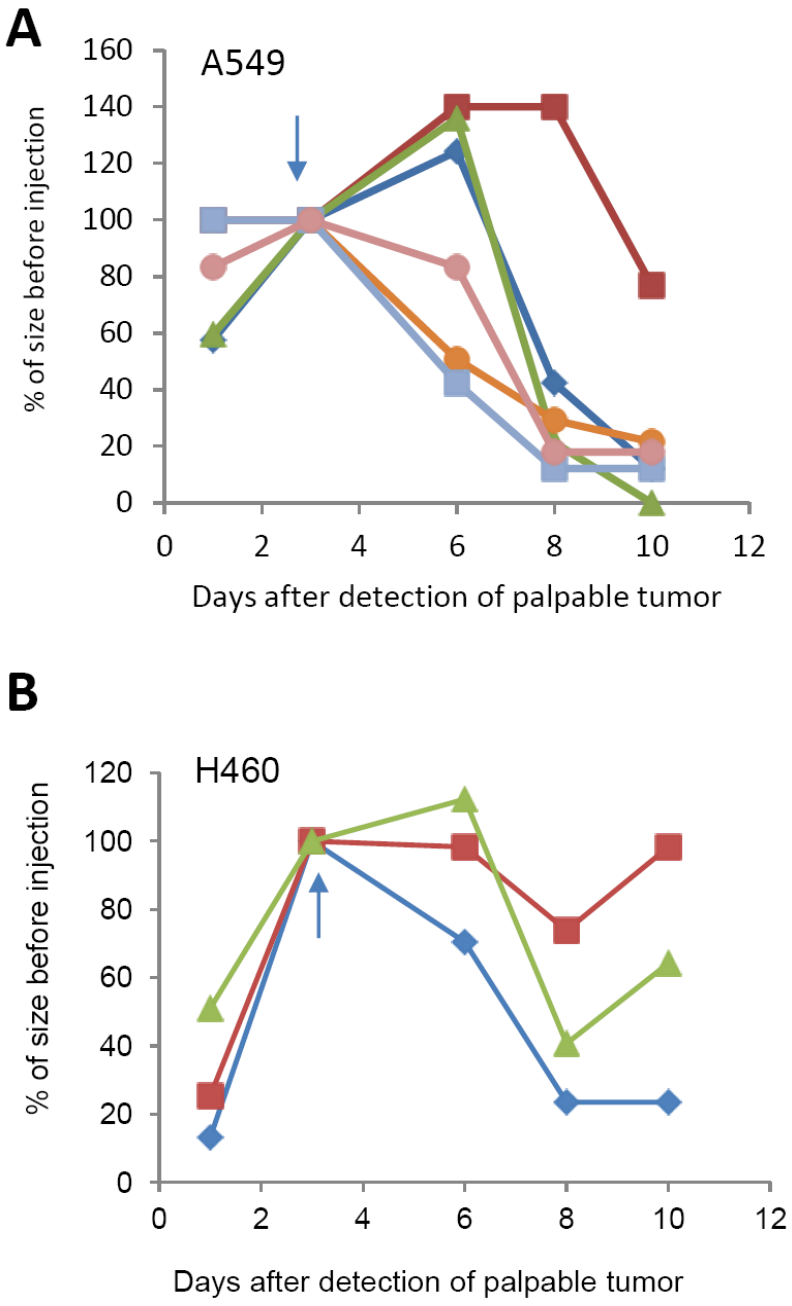

Fig. S10. Effect of CMA blockage on growth of pre-formed human lung cancer cell tumors.

Growth curves of individual tumors grown from xenografts of A549 (**A**) and H460 (**B**) human lung cancer cells to sizes of up to 100-200 mm^3 and directly injected with lentivirus carrying shRNA against LAMP-2A on two consecutive days. Values show rates of tumor growth relative

to the size of the tumor at first injection. Three different tumors for each group are shown. Arrows indicate time of injection.

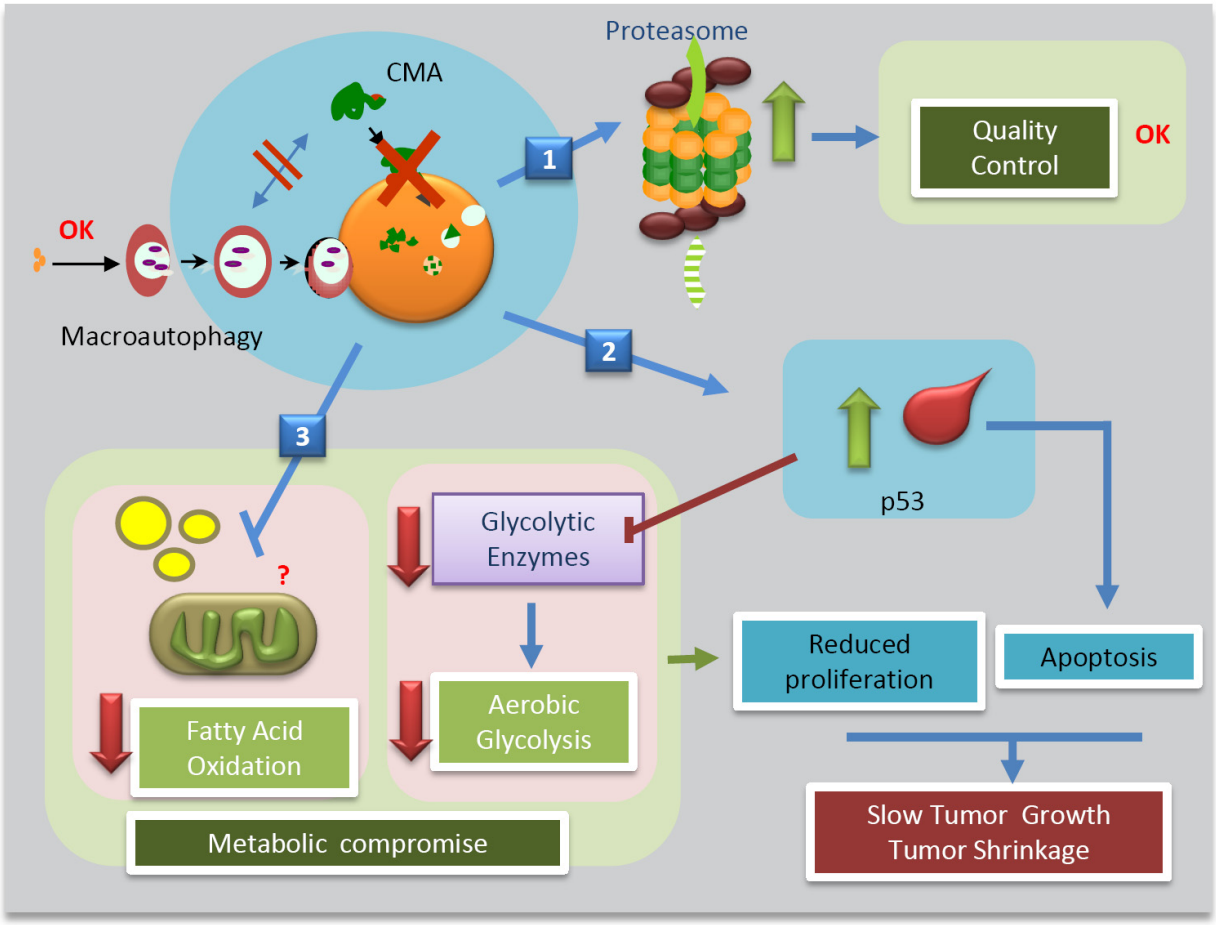

Fig. S11. Hypothetical model of the consequences of CMA inhibition in cancer cells. The cancer cells analyzed in this study do not respond to CMA blockage with upregulation of macroautophagy but they increase rates of proteasome-dependent degradation, which allows maintenance of proper cellular quality control. Blockage of CMA increases cancer cell death and reduces their proliferation, in part, through changes in different metabolic pathways. The observed increase in p53 in the CMA-compromised cells is responsible for the reduced glycolytic activity in these cells, and this along with the reduction in mitochondria β-oxidation may contribute to the reduced rates of proliferation. Blockage of CMA slows down tumor growth and reduces size of pre-formed tumors through a combined effect on cellular proliferation and viability.

References

1. A. M. Cuervo, J. F. Dice, A RECEPTOR FOR THE SELECTIVE UPTAKE AND DEGRADATION OF PROTEINS BY LYSOSOMES, *Science* **273**, 501-503 (1996).
2. F. Aniento, A. G. Papavassiliou, E. Knecht, E. Roche, SELECTIVE UPTAKE AND DEGRADATION OF C-FOS AND V-FOS BY RAT LIVER LYSOSOMES, *FEBS Lett* **390**, 47-52 (1996).
3. A. C. Massey, S. Kaushik, G. Sovak, R. Kiffin, A. M. Cuervo, CONSEQUENCES OF THE SELECTIVE BLOCKAGE OF CHAPERONE-MEDIATED AUTOPHAGY, *Proc Nat Acad Sci USA* **103**, 5905-5910 (2006).
4. M. Martinez-Vicente, Z. Talloczy, E. Wong, G. M. Tang, H. Koga, S. Kaushik, R. de Vries, E. Arias, S. Harris, D. Sulzer, A. M. Cuervo, CARGO RECOGNITION FAILURE IS RESPONSIBLE FOR INEFFICIENT AUTOPHAGY IN HUNTINGTON'S DISEASE, *Nature Neuroscience* **13**, 567-U574 (2010).
5. U. Bandyopadhyay, S. Sridhar, S. Kaushik, R. Kiffin, A. M. Cuervo, IDENTIFICATION OF REGULATORS OF CHAPERONE-NEDIATED AUTOPHAGY, *Mol Cell* **39**, 535-547 (2010).
6. S. Kaushik, A. M. Cuervo, METHODS TO MONITOR CHAPERONE-MEDIATED AUTOPHAGY, *Methods Enzymol* **452**, 297-324 (2009).
7. H. Koga, M. Martinez-Vicente, V. V. Verkhusha, A. M. Cuervo, A PHOTOCONVERTIBLE FLUORESCENT REPORTER TO TRACK CHAPERONE-MEDIATED AUTOPHAGY, *Nat. Comm.* **2**, 386 (2011).
8. A. Follenzi, L. Naldini, GENERATION OF HIV-1 DERIVED LENTIVIRAL VECTORS., *Methods Enzymol* **346**, 454-465 (2002).
9. T. T. Koll, S. S. Feis, M. H. Wright, M. M. Teniola, M. M. Richardson, A. I. Robles, J. Bradsher, J. Capala, L. Varticovski, HSP90 INHIBITOR, DMAG, SYNERGIZES WITH RADIATION OF LUNG CANCER CELLS BY INTERFERING WITH BASE EXCISION AND ATM-MEDIATED DNA REPAIR, *Mol Cancer Ther* **7**, 1985-1992 (2008).

10. C. Hoppel, J. P. DiMarco, B. Tandler, RIBOFLAVIN AND RAT HEPATIC CELL STRUCTURE AND FUNCTION. MITOCHONDRIAL OXIDATIVE METABOLISM IN DEFICIENCY STATES. , *J. Biol. Chem.* **254**, 4164–4170 (1979).

11. C. Zhang, A. M. Cuervo, RESTORATION OF CHAPERONE-MEDIATED AUTOPHAGY IN AGING LIVER IMPROVES CELLULAR MAINTENANCE AND HEPATIC FUNCTION., *Nat Med* **14**, 959-965 (2008).